THE JOURNAL OF BIOLOGICAL CHEMISTRY
Vol. 277, No. 46, Issue of November 15, pp. 43948–43960, 2002
Printed in U.S.A.

The Metabolic Architecture of Plant Cells

STABILITY OF CENTRAL METABOLISM AND FLEXIBILITY OF ANABOLIC PATHWAYS DURING THE GROWTH CYCLE OF TOMATO CELLS*

Received for publication, June 26, 2002, and in revised form, August 23, 2002
Published, JBC Papers in Press, September 10, 2002, DOI 10.1074/jbc.M206366200

Denis Rontein‡§, Martine Dieuaide-Noubhani‡, Erick J. Dufourc¶, Philippe Raymond‡, and Dominique Rolin‡‖

From the ‡UMR 619, Biotechnologie et Physiologie Végétales, Institut de Biologie Végétale et Moléculaire, Institut National de la Recherche Agronomique, Bordeaux, BP 81, Villenave d'Ornon 33883 cedex and the ¶Institut Européen de Chimie et Biologie, Ecole Polytechnique, Ave. Pey Berland, BP 108, Talence 33402, France

The changes in the intermediary metabolism of plant cells were quantified according to growth conditions at three different stages of the growth cycle of tomato cell suspension. Eighteen fluxes of central metabolism were calculated from ^{13}C enrichments after near steady-state labeling by a metabolic model similar to that described in Dieuaide-Noubhani *et al.* (Dieuaide-Noubhani, M., Raffard, G., Canioni, P., Pradet, A., and Raymond, P. (1995) *J. Biol. Chem.* 270, 13147–13159), and 10 net fluxes were obtained directly from end-product accumulation rates. The absolute flux values of central metabolic pathways gradually slowed down with the decrease of glucose influx into the cells. However, the relative fluxes of glycolysis, the pentose-P pathway, and the tricarboxylic acid cycle remained unchanged during the culture cycle at 70, 28, and 40% of glucose influx, respectively, and the futile cycle of sucrose remained high at about 6-fold the glucose influx, independently from carbon nutritional conditions. This natural resistance to flux alterations is referred to as metabolic stability. The numerous anabolic pathways, including starch synthesis, hexose accumulation, biosynthesis of wall polysaccharides, and amino and organic acid biosynthesis were comparatively low and variable. The phosphoenolpyruvate carboxylase flux decreased 5-fold in absolute terms and 2-fold in relation to the glucose influx rate during the culture cycle. We conclude that anabolic fluxes constitute the flexible part of plant cell metabolism that can fluctuate in relation to cell demands for growth.

Plants are able to grow under a wide range of environmental conditions (extreme temperatures, insufficient or excessive light, and shortage of water or mineral nutrients) and show a robust physiological homeostasis. To ensure this homeostasis, plant metabolism has to be very flexible (1). In all cells, the central carbon metabolism provides energy, cofactor regeneration, and building blocks for biomass and secondary metabolism. The flexibility of plant metabolism, which is probably an evolutionary adaptation to the variable environmental conditions plants normally experience, has been explained by the buffering effect of carbon storage and allocation (2) and by the complexity of regulation or built-in redundancy owing to alternative enzymes and pathways for many processes (3). For example, parallel glycolytic pathways are present in the cytosol and plastid; in the cytosol, the classic key sites for regulation of glycolysis at phosphofructokinase and pyruvate kinase (PK)[1] can be bypassed by pyrophosphate:fructose-6-phosphate phosphotransferase and phosphoenolpyruvate carboxylase (PEPC) (3).

The development of genetic engineering, which introduced a new dimension to pathway knowledge by allowing precise modifications of specific enzymatic reactions in metabolic pathways, also highlighted the flexibility of plant primary metabolism (4–6). Pyrophosphate:fructose-6-phosphate phosphotransferase and cytosolic PK, which generally have been considered essential, were almost removed without any significant effect on growth or development (7–9). In contrast, in yeast many genes encoding glycolytic enzymes (*e.g.* hexose kinase, phosphoglucose isomerase, phosphoglucose kinase, PK, and alcohol dehydrogenase) have been overexpressed many times, but in none of the mutants did the glycolytic flux differ substantially from the wild type flux (10, 11). In plants, overexpression of the spinach choline monooxygenase gene in tobacco chloroplasts did not contribute to the accumulation of glycine betaine (12). This inherent resistance to flux alteration by genetic manipulation, which was designed to enhance the yield in biosynthetic choline pathways, has also been named "rigidity" (13). The concept of "network rigidity" was initially proposed by Stephanopoulos and Vallino (14) and was considered to result from mechanisms that stabilize flux ratios at branch points in metabolic networks. The enzymes bifurcating from a rigid node are activated by intermediates in the opposite branch. The interdependency of enzyme activities in competing branches stabilizes the ratio of branching fluxes and maintains flux distribution, which is optimal for growth. In view of carbon metabolism adaptations in response to environmental changes in plants, the following question can be raised: does the plant primary metabolism coordinate a relatively uniform constant distribution of building block metabolites and energy or does it support radically different flux distributions in response to different environmental stimuli?

A variety of methods have been developed to quantify intracellular fluxes in animals (15, 16), microorganisms (17), and plants (18–23). Radio or stable isotopic tracers such as ^{14}C or ^{13}C can be used according to three major methods (22). A

* This work was supported in part by grants from the Institut National de la Recherche Agronomique (INRA), the Université Victor Segalen Bordeaux 2, and the Conseil Régional d'Aquitaine. The costs of publication of this article were defrayed in part by the payment of page charges. This article must therefore be hereby marked "*advertisement*" in accordance with 18 U.S.C. Section 1734 solely to indicate this fact.

§ Supported by a doctoral fellowship from the Ministère de l'Education Nationale de la Recherche et de la Technologie.

‖ To whom correspondence should be addressed. Tel.: 33-5-57-12-26-90; Fax: 33-5-57-12-25-41; E-mail: rolin@bordeaux.inra.fr.

[1] The abbreviations used are: PK, pyruvate kinase; PEPC, phosphoenolpyruvate carboxylase; HPLC, high-performance liquid chromatography; SR, specific radioactivity; FW, fresh weight; DW, dry weight; PPP, pentose-phosphate pathway.

commonly used method is to calculate a flux from the rate of end-product labeling and the specific radioactivity of the precursor (23). Alternatively, tissues are labeled to isotopic steady state, and intermediate labeling can be used for flux calculation using a linear equation, independently of time (18, 20, 24). Fluxes can also be measured directly by *in vivo* NMR using the techniques of magnetization transfers (21). In plants, major fluxes of carbohydrate metabolism have been estimated during starch breakdown by ripening bananas (23), during carbon starvation (20, 25), during hypoxia in corn root tips (21, 26), and in early germinating lettuce seeds (18). Dieuaide-Noubhani *et al.* (20, 25) identified and quantified 20 metabolic fluxes from sucrose turnover to input into the tricarboxylic acid cycle in maize root tips. Changes observed in the enrichments of intermediary metabolites during the first stages of sugar starvation indicated that sugar nutrition profoundly affects the metabolic network in excised corn root tips. Acetyl-CoA entering the tricarboxylic acid cycle is progressively supplied by lipids and proteins, and the anaplerotic flux through the PEPC vanishes long before carbohydrates are exhausted.

The aim of the present work was to examine changes in fluxes of intermediary metabolism in heterotrophic plant cells in suspension cultures, in response to changes in the culture medium and growth stages during a growth cycle. Tomato cells were labeled to the isotopic steady state with [1-^{13}C]glucose. ^{1}H and ^{13}C NMR were used to determine ^{13}C enrichments of specific carbons of carbohydrates and amino acids. Metabolic pathway modeling was used to interpret isotope distribution according to Ref. 20. Using these data, 29 metabolic fluxes were quantified at 3 different physiological stages during the growth cycle of tomato cells. The results show the following: (i) That relative fluxes in the central metabolism (glycolysis, tricarboxylic acid cycle, and pentose-P pathway) and futile cycles (sucrose turnover and triose-P to hexose-P recycling) are high and stable. (ii) On the contrary, relative fluxes in anabolic pathways, such as the anaplerotic flux catalyzed by PEP carboxylase, are low and variable, constituting the flexible part of metabolism, which may fluctuate to fit precursor availability for the anabolic pathway in relation to cell needs.

EXPERIMENTAL PROCEDURES

Growth of Tomato Suspension Cells—Cells of *Lycopersicon esculentum cerasiformae sweet 100* obtained from J.-L. Montillet (Cadarache, France) were grown in MS medium (27) containing 166 mM glucose instead of sucrose, in continuous darkness in a rotary shaker (Infors AG, Bootmingen, Switzerland) 150 rpm at 23 °C. Cells were subcultured every 5 days by diluting 10 ml of packed cells in 90 ml of fresh medium in 250-ml Erlenmeyer flasks. At this time (time 0) the cell density was 60 mg fresh weight (FW).ml^{-1}. Cells were harvested by filtration on paper disks, briefly washed with water, frozen in liquid nitrogen, and stored at −80 °C.

Labeling to Isotopic and Metabolic Steady States during the Growth Cycle—For ^{14}C labeling, cells were subcultured in medium containing 166 mM [1-^{14}C]glucose (25 dpm/nmol). In ^{13}C labeling, 166 mM [1-^{13}C]glucose was used. The absolute enrichment of [1-^{13}C]glucose in the medium, as measured by ^{1}H NMR was 92% on carbon 1 at all time points. Other glucose carbons were not labeled, *i.e.* their natural enrichment was 1.1%. The metabolic network of the cells was studied at three stages corresponding to three different physiological situations: (i) day 5 (exponential phase), (ii) day 6 (arrest of cell divisions), and (iii) day 7.5 (pre-stationary phase).

Labeling with [U-^{14}C]Leucine—Cells were subcultured in the MS medium containing 166 mM glucose plus [U-^{14}C]leucine (146 kBq.50 ml^{-1}, 10.9 GBq.mmol^{-1}). In parallel, other cells were subcultured in the MS medium without labeled leucine to prepare a chase medium. After 3 days, cells were washed (5×) and transferred to the chase medium. Samples were collected at the time indicated up to day 7.

Analysis of Metabolites—The extraction of soluble cell components (500 mg of FW) was performed using boiling aqueous solutions of ethanol, as previously described (28). The water-soluble compounds were dried, dissolved in water (500 μl), and used to separate sugars, amino acids, and organic acids. Starch contained in the pellet at the last stage of the alcoholic extraction was washed, converted to glucose (29), and measured as glucose, as described below. The remaining pellets were freeze-dried. The dry weight of this residue was representative of the insoluble macromolecules from the cell wall. Enzymatic assays of glucose, fructose, sucrose (30), and citric and malic acids (31) were adapted for an MR 5000 microplate reader (Dynatech, St. Cloud, France). Amino acids were analyzed by reverse phase HPLC (Thermo Separation Products, Riviera Beach, FL) on a C18 column after AccQ-Tag derivatization (32). Detection was performed with a TSP-fl 3000 fluorescence detector with excitation at 250 nm and emission at 394 nm. Amino acid quantification was achieved with the Millennium 2.15 software (Waters). Calibration was performed using an AAS18 solution of amino acid standards from Sigma (St. Louis, MO).

Labeling Determination—For sugars, the water-soluble extract was deionized using anion and cation exchange resins and analyzed by HPLC on an Aminex HPX-87C column (Bio-Rad) as described previously (29). Each peak was collected and counted, and the specific radioactivity was determined. Amino acid fractions were isolated by ion exchange chromatography (18) and analyzed by HPLC after derivation with *o*-phthaldialdehyde (33), and the specific radioactivity of each amino acid was determined as in a previous study (18). For ^{13}C NMR analysis, aspartate, glutamate, and the amino mono-acid fraction containing alanine were purified by ion-exchange chromatography from the total soluble extract as described (18, 20). Ala was further purified through an AG 50W X8 100–200 mesh (H^+) column, after isocratic elution with 1 N HCl. The last two fractions were freeze-dried several times to eliminate residual acetate.

Protein Determination—Total proteins were extracted with the following buffer: 50 mM Tris-HCl, pH 7.5, 1% (w/v) SDS, 5 mM sodium ascorbate, 0.3 mM EDTA. Cells were crushed in a mortar with liquid nitrogen and 0.5% (w/w) polyvinyl polypyrrolidone. After centrifugation (20,000 × *g*, 40 min), the supernatants were analyzed for protein using the Bio-Rad DC (detergent compatible) protein assay with bovine serum albumin as standard.

Amino Acid Composition of Proteins—The extracted proteins were precipitated with 10% trichloro-acetic acid (w/v) and centrifuged at 10,000 × *g* for 10 min before hydrolysis with 6 N HCl at 110 °C in sealed tubes. Amino acids were analyzed by HPLC using the AccQ method (32). For the determination of the specific radioactivity of Leu, amino acids were analyzed by HPLC after derivation with *o*-phthaldialdehyde (33).

NMR Analysis—NMR analyses were performed at 24 °C with a 9.4 T Bruker Avance 400 spectrometer equipped with a 5-mm QNP probe and deuterium lock. ^{1}H and ^{13}C NMR spectra were obtained at 400.13 and 100.61 MHz using a Hahn echo (34) and a recycling time greater than 6 T_1. For glucose, sucrose, Glu and Ala, T_1 was measured with an inversion-recovery sequence and found to be, respectively, 1.5, 0.7, 2.2, and 4.3 s for ^{1}H and 0.9, 0.9, not determined, and 2 s ^{13}C NMR. The spectra represent the longest T_1 for the molecule of interest. WALTZ-16 proton decoupling was performed during ^{13}C NMR acquisition. Prior to Fourier transformation, ^{13}C- and ^{1}H-free induction decays were zero-filled once to improve digital resolution and multiplied by an exponential function to improve the signal-to-noise ratio (16,000 and 32,000 points, 3- and 0.3-Hz line broadening for ^{13}C and ^{1}H NMR spectra, respectively). Peak assignment was performed according to a previous study (20) and from spectra of pure compounds.

The absolute ^{13}C enrichments of the Glu carbons C-2, C-3, and C-4; Ala C-3; and glucose α and β C-1, sucrose glucosyl C-1, and starch glucosyl C-1 were determined from ^{1}H NMR spectra, as the ratio of the area of the satellites (^{1}H-^{13}C J-coupling) to the total area of the multiplet. Spectral integration was accomplished with stepped integrals. The relative enrichments of the glucose and sucrose carbons C-2 to C-6 were determined by ^{13}C NMR in comparison with the absolute enrichment of glucose and sucrose glucosyl C-1 measured by ^{1}H NMR. The same method was used to determine the relative enrichment of Ala C-2 from the absolute enrichment of Ala C-3.

Chemicals—[1-^{14}C]Glucose (1.856 GBq/mmol) was obtained from Amersham Biosciences (Les Ulis, France), and [1-^{13}C]glucose (99% enrichment) was from Isotec (St. Quentin, France). Protease from *Streptomyces griseus* (Pronase) was purchased from Sigma (St. Quentin, France). Yeast hexokinase, *Leuconostoc* glucose-6-P dehydrogenase, invertase, and yeast glucose-6-P isomerase were obtained from Sigma (St. Quentin, France). Analytical grade mineral salts and *Aspergillus* amyloglucosidase were purchased from Merck (Darmstadt, Germany).

Calculations—Equations were written according to Ref. 24. The resolution of simultaneous algebraic equations (see "Appendix") was performed using the software Mathematica (Wolfram Research, Champaign, IL).

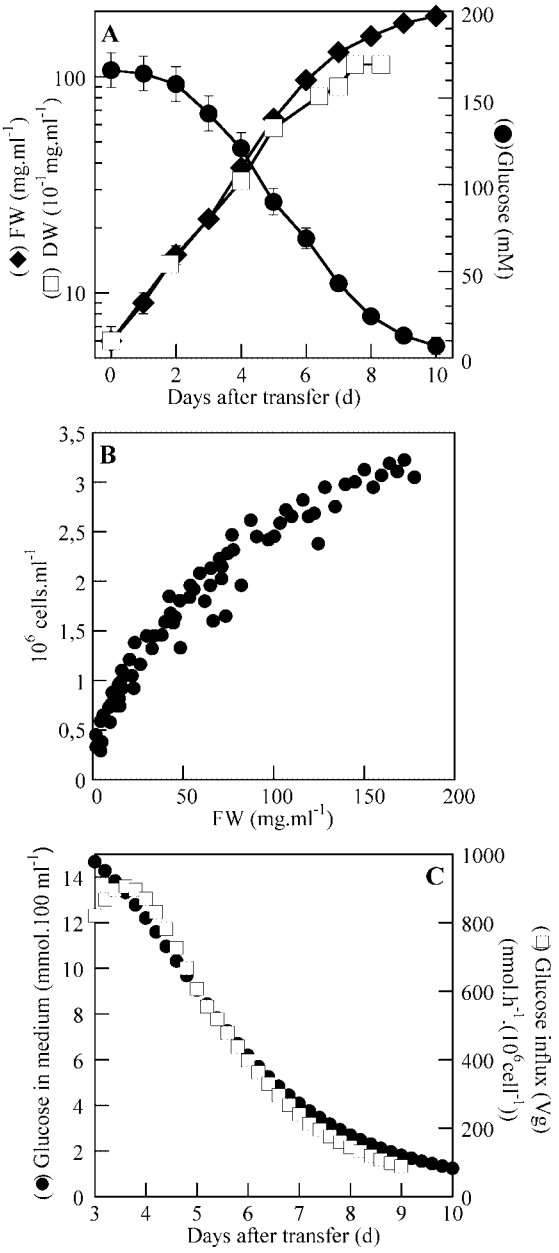

FIG. 1. **Tomato cell growth in the MS medium with glucose as a carbon source.** *A*, changes in FW (♦) and DW (□), and concomitant decrease in glucose concentration (●) in the medium. Tomato cells were cultivated in MS medium, and glucose concentration was determined by enzymatic assay (see "Experimental Procedures"). *Abscissa*, days in culture after transfer to fresh medium. *Vertical bars* represent the S.D. of the mean from four independent experiments. *B*, cell counting (●). Before cell counting, cells were dissociated by cellulase and pectolyase. *C*, glucose influx (Vg) (□). This influx was calculated from the rate of glucose uptake (*A*) taking into account the number of cells present in the medium (*B*) during the cell growth cycle. The time course of glucose concentration in the medium (●) was adjusted by a sigmoid equation with the Kaleidagraph software. The adjustment points were plotted with a 0.2-day period. The first derivative relative to time was calculated and adjusted to the number of the cells present at each time.

RESULTS

Cell Growth, Glucose Uptake, and Cellular Metabolite Content

The growth rate of tomato cells in liquid culture was established by measuring fresh weight (FW), dry weight (DW), and cell number (Fig. 1, *A* and *B*). The growth curve profile was similar to that of most other plant cell cultures (35, 36). Growth was exponential during the first 6 days after subculture. Fig. 1*A* indicates that, after day 5, FW increased more by cell enlargement than by cell division. This was confirmed by the decrease in the rate of [^{3}H]thymidine incorporation into DNA from day 4, and the disappearance of cyclin A_2 and D_3 mRNA at day 5, thus indicating the arrest of cell division (data not shown). In batch culture, most physical and chemical conditions change during the growth cycle. In our experiment, glucose disappeared from the medium in a sigmoid fashion (Fig. 1*A*). The glucose influx rate (Vg) decreased in parallel, from 903 ± 45 at day 3 to 180 nmol.h^{-1}.(10^6 cells)$^{-1}$ at day 7.5 (Fig. 1*C*). At day 6, nitrogen (NH_4^+, 15 mM) and glucose (65 mM) were still available in the culture medium, whereas inorganic phosphate measured by the molybdate method was under 0.02 mM. The vacuolar phosphate was not detectable by *in vivo* ^{31}P NMR, but the cytoplasmic P_i level was the same as on day 1 (data not shown). No P_i starvation symptom was observed. Growth (FW curve) slowed down after day 6 and stopped after day 10 when glucose was exhausted from the medium (Fig. 1*A*).

During a culture cycle, 70% of the absorbed glucose was used to sustain respiration. The main end products of glucose metabolism accumulated during a growth cycle (*i.e.* soluble and insoluble sugars, organic acids, and proteins) are shown in Fig. 2. Soluble sugars mainly accumulated at the end of the exponential phase between days 5 and 6 (Fig. 2*A*). At the end of the culture, the accumulation of cell wall polysaccharides, soluble sugars, and starch was, respectively, 1.7, 1.2, and 0.6 mmol of glucose equivalent per flask corresponding to 10, 8, and 4% of the initial glucose (Fig. 2, *A* and *B*). The organic acid content (0.1 mmol per flask at the end of the culture, Fig. 2*C*) was a small fraction of accumulated carbon. Citrate and malate mainly accumulated after day 5 when cell growth started to decline (Fig. 2*C*). Total proteins constantly increased during the cell growth cycle (Fig. 2*D*). Their amino acid composition remained stable during the growth cycle. The carbon flux for each group of amino acids contributing to protein accumulation was calculated from the rate of protein accumulation (Fig. 2*D*) and the established pathway of amino acid biosynthesis (Fig. 3) (37, 38).

The fluxes to fatty acid and nucleic acid synthesis were minor and not included in the model. In tomato cell suspensions, nucleic acids (DNA-RNA) were estimated to be 1 μg.(10^6 cells)$^{-1}$, which corresponds to a relative flux of pentose-P into the nucleic acids equal to only 0.1% of the glucose influx.

Carbohydrate and Amino Acid Enrichments Measured by ^{1}H and ^{13}C NMR

The time needed to reach the isotopic and metabolic steady state was determined as in a previous study (20) by monitoring the evolution of $^{14}CO_2$ and the specific radioactivity of cellular soluble sugars, starch, Ala, and Glu. The soluble sugars and amino acids were near isotopic steady state after 3 and 4 days, respectively (data not shown).

Typical ^{13}C and ^{1}H NMR spectra of purified glucose, sucrose, and starch from tomato cells after 5 days of culture with [1-^{13}C]glucose are shown in Fig. 4. The resonance assigned to glucose, fructose, and sucrose are clearly visible. The highest amounts of ^{13}C were at C-1 of α and β free glucose (Fig. 4*A*), C-1 of glucosyl and fructosyl moieties of sucrose (Fig. 4*B*), and C-1 of α and β glucose deriving from starch hydrolysis (Fig. 4*C*). The spectra also showed appreciably more labeling at C-6 than at the other carbons (except C-1) of these hexose residues. The carbon enrichment values of these sugars are presented in Table I.

^{1}H and ^{13}C NMR spectra of Glu and Ala are presented in Fig. 5, and enrichments are shown in Table II. Glu, C-2, and C-3

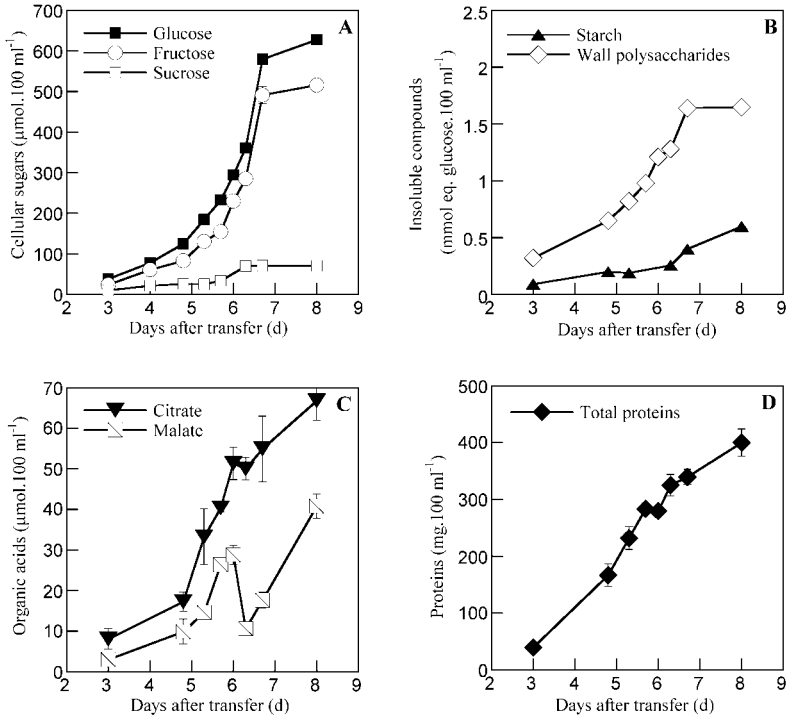

FIG. 2. **Changes in soluble sugars (*A*), insoluble compounds (*B*), organic acids (*C*), and total proteins (*D*), during the cell growth cycle.** Sugars and organic acids were determined by enzymatic assay, proteins by Bio-Rad DC assay as described under "Experimental Procedures." Cell wall polysaccharides were determined from insoluble compounds after ethanolic extraction and starch digestion of the cells. *Abscissa*, days in culture after transfer to fresh medium. *Vertical bars* represent the S.D. of the mean from four samples in two independent experiments.

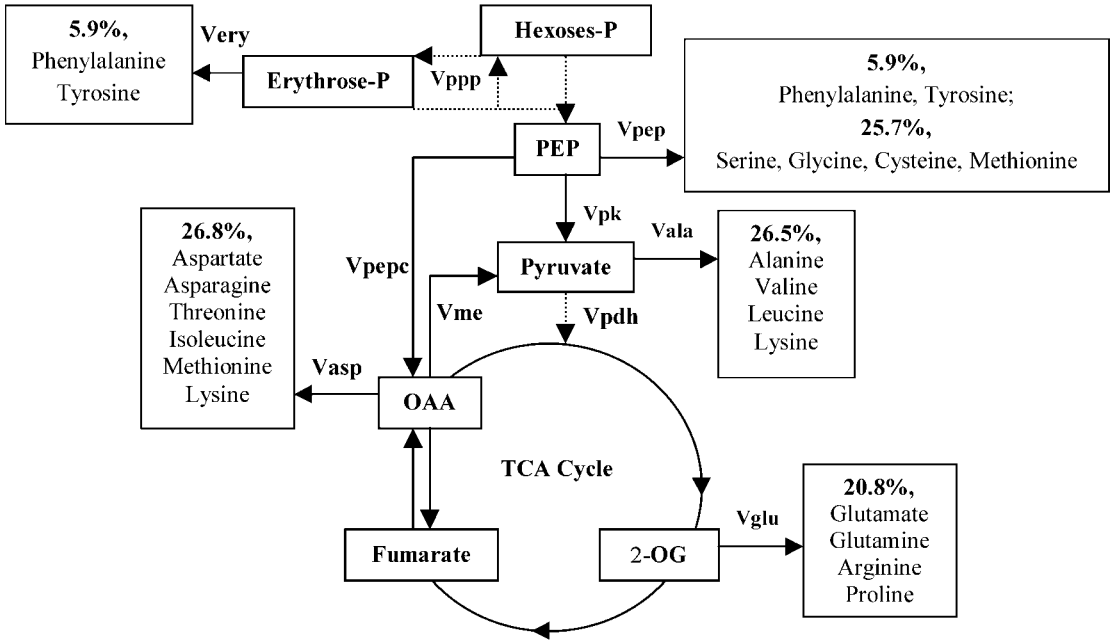

FIG. 3. **Biosynthetic pathways of amino acid groups connected to central metabolism and amino acid compositions of total proteins in tomato cells.** Amino acid biosynthesis from 2-OG (Vglu), OAA (Vasp), pyruvate + acetyl-CoA (Vala), PEP (Vpep), and erythrose-P (Very) are shown. The numbers represent the amino acid percentage for each metabolic group in total proteins. The sum of the amino acid percentages is superior to 100% because some amino acids belong to several groups. Amino acids are determined after acid hydrolysis and HPLC analysis under "Experimental Procedures." Results are the mean of two experiments in each of the three physiological conditions as described under "Experimental Procedures."

have similar enrichment values at about 75% of the C-4 enrichment. The ^{13}C enrichment of Ala C-3 was close to that of Glu C-4. Ala C-2 enrichment was just above background.

Modeling the Metabolic Network

The metabolic scheme that accounts for tracer distribution is essentially similar to that developed in Ref. 20, with some modifications described below and shown in Fig. 6.

Sugar Metabolism—The label distributions observed in the glucosyl and fructosyl moieties of sucrose were similar. It was therefore assumed that the cytosolic hexose-P constituted a single pool (Fig. 6). The labeling of intracellular free glucose C-6 suggested that part of intracellular glucose was formed from hexose-P via a sucrose cycle (Vi) (Fig. 6). According to Ref. 20, the C-6 enrichment of the hexose-P pool can be explained by both triose-P recycling and exchange through the cytosolic transaldolase reaction (Vtald) (Fig. 6). The absence of detectable label in free glucose C-2 and C-5 suggests the absence of gluconeogenesis (Fig. 6). The fact that the total enrichment (C-1 + C-6) of free glucose, sucrose, and starch glucosyl was

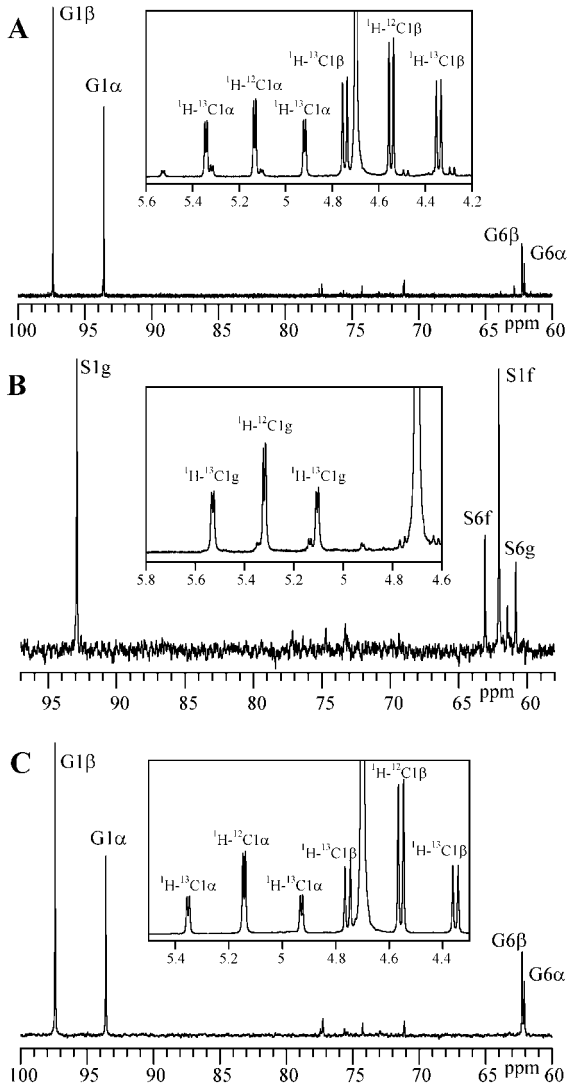

FIG. 4. **^{13}C and ^{1}H (*inset*) NMR spectra of glucose (*A*), sucrose (*B*), and glucose from starch hydrolysate (*C*).** Tomato cells were fed with [1-^{13}C]glucose for 5 days. Cellular sugars were purified by HPLC as described under "Experimental Procedures." Starch was extracted and hydrolyzed to glucose. The terms *Gi*α and *Gi*β indicate the resonance of carbon *i* of α and β glucose. The terms *Sig* and *Sif* indicate the resonance of carbon *i* of glucosyl and fructosyl moieties. ^{1}H and ^{13}C spectra represent the accumulation of 128 and 256 scans, respectively.

TABLE I

Steady-state enrichments of carbohydrates of cultured tomato cells with [1-^{13}C]glucose during exponential phase (day 5), arrest of cell division (d 6), and pre-stationary phase (day 7.5)

The enrichments (in percent) were determined from ^{1}H and ^{13}C spectra as described under "Experimental Procedures." Results are given as mean ± S.D. (n = 2) taking into account the error associated with the integration measurements. Statistical significance was evaluated by using Fisher-Student's test analysis as appropriate (p = 0.05); the results are indicated by *subscript letter* for significant different value.

	^{13}C enrichment		
	Glucose	Sucrose glucosyl	Starch glucosyl
	%		
Day 5			
C-1	$61.3 \pm 0.3_a$	$56.6 \pm 1_c$	$48.5 \pm 0.5_e$
C-6	$16.1 \pm 0.5_b$	$17 \pm 1.3_d$	$17.1 \pm 0.8_d$
Day 6			
C-1	$61.2 \pm 0.3_a$	$56 \pm 1_c$	$50 \pm 1.5_f$
C-6	$16.6 \pm 0.5_b$	$18.2 \pm 1.5_d$	$17.8 \pm 1.8_d$
Day 7.5			
C-1	$61.6 \pm 0.3_a$	$56.1 \pm 1.2_c$	$53.4 \pm 1.1_h$
C-6	$18.6 \pm 0.6_g$	$18.6 \pm 1.8_d$	$20 \pm 1.4_i$

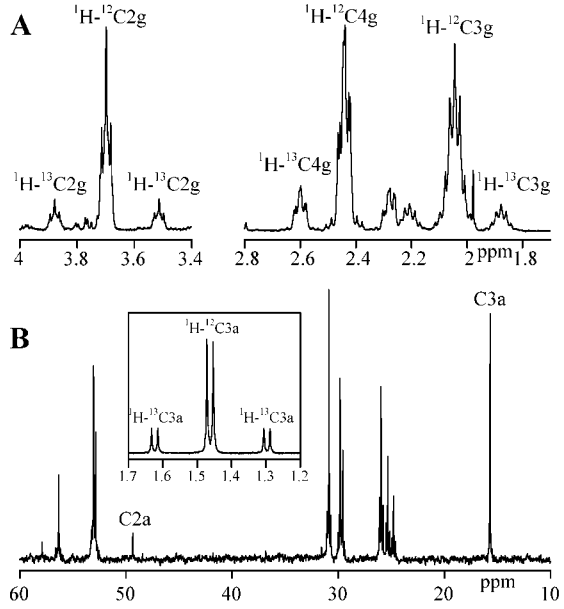

FIG. 5. **^{1}H (*top* and *inset*) and ^{13}C-NMR spectra of Glu (*A*) and Ala (*B*).** Tomato cells were fed with [1-^{13}C]glucose for 5 days. Amino acids were purified by cation exchange resin as described under "Experimental Procedures." The terms *Cig* indicate the resonance of carbon *i* of Glu and *Cia* the resonance of carbon *i* of Ala. ^{1}H and ^{13}C spectra represent the accumulation of 128 and 1800 scans, respectively.

gradually lower than that of the glucose precursor (92%) was accounted for by the pentose-P pathway (Vppp), the only possibility in the absence of gluconeogenesis (Fig. 6). The similar enrichments of starch glucosyl C-6, and sucrose glucosyl C-6 (Table I) indicated that starch was essentially formed from hexose-P imported from the cytosol with no further exchange of hexose-P C-6 with triose-P C-1. This was not the case in corn root tips (20) and suggested an exchange between the plastidial and cytosolic hexose-P. This is shown in the present model as a reverse flux (Vhpc) of hexose-P from plastids to cytosol (Fig. 6). The hexose-P exchange between cytosol and plastids could be performed either by a hexose-P translocator of the plastid double membrane, as suggested recently (39), or by a glucose translocator (40). The lower enrichment of the starch glucosyl C-1 compared with cytosolic hexose-P C-1 (Table I) indicated the occurrence of a flux through the plastidial PPP, with recycling of C-1 unlabeled hexose-P inside plastids. As in Ref. 20, the cytosolic and plastidial triose-P were assumed to be in rapid exchange, and only one pool was considered.

Anaplerotic and Respiratory Carbon Fluxes through the Tricarboxylic Acid Cycle—The glycolytic flux (Vgly) measured on the linear pathway between triose-P and PEP is split between the oxidative flux through PK, the anaplerotic flux through PEPC, which is the main source of four carbon compounds in the tricarboxylic acid cycle, and amino acid biosynthesis using PEP as precursor (Fig. 6). According to (18, 20), the anaplerotic flux leads to the dilution of C-2 and C-3 enrichments compared with C-4 enrichment of Glu, thus allowing the quantification of the relative flux through the oxidative *versus* anaplerotic pathways (Table II). The identical enrichment of Glu C-4 and Ala C-3 (Table II) indicated that there was no diluting flux between pyruvate and Glu, *i.e.* glycolysis was the only source of acetyl CoA. The low enrichment of C-2 Ala showed the occurrence of a relatively small

TABLE II
Steady-state enrichments of amino acids during exponential phase (day 5), arrest of cell division (day 6), and pre-stationary phase (day 7.5)

The enrichments (in percent) were determined from ^{1}H and ^{13}C spectra as described under "Experimental Procedures." Results are given as mean ± S.D. ($n = 2$) taking into account the error associated with the integration measurements. Statistical significance was evaluated by using the Fisher-Student test analysis as appropriate ($p = 0.05$); the results are indicated by *subscript letter* for significant different values.

	^{13}C enrichment	
	Alanine	Glutamate
	%	
Day 5		
C-2	$2.3 \pm 0.4_j$	$24.2 \pm 0.3_l$
C-3	$30.4 \pm 0.2_k$	$22.4 \pm 0.4_m$
C-4		$30.5 \pm 0.2_k$
Day 6		
C-2	$3 \pm 1_j$	$25 \pm 0.4_n$
C-3	$30.6 \pm 0.2_k$	$23.4 \pm 0.4_o$
C-4		$30.8 \pm 0.6_k$
Day 7.5		
C-2	$2.1 \pm 0.4_j$	$27.2 \pm 0.4_q$
C-3	$31 \pm 0.2_p$	$25.8 \pm 0.4_r$
C-4		$31.6 \pm 0.2_s$

flux from malate to Ala through the malic enzyme reaction (Fig. 6).

Amino Acid Fluxes—Our model also includes the fluxes of amino acid biosynthesis calculated from the rate of amino acid accumulation into total proteins (Fig. 2*D*). During the culture cycle, the amino acid composition of total protein remained constant (Fig. 3). Table III presents the conversion factor (*F*) used to calculate the fluxes (Vx) related to each amino acid group.

Validation of the Model

The metabolic network presented in Fig. 6 is composed of 29 fluxes. The enrichment values shown in Tables I and II were used to calculate the relative values of 18 metabolic fluxes as a percentage of the glucose influx rate using the mathematical model shown under "Appendix" (Table IV). The validity of the model was tested by comparing calculated values given by the model with experimental values obtained in independent experiments.

Steady State and Memory Effects—The model describing metabolic and isotopic steady state implies that the reaction rates and the ^{13}C enrichment of metabolites are constant over time. Isotopic steady state was reached after 3 days for free hexoses and 4 days for amino acids (data not shown). In the course of the culture, however, the enrichments (Tables I and II) and flux values (Table IV) changed constantly. Therefore the following question arises: do the enrichment values of a metabolite reflect flux values at the sampling time? We assumed that quasi-steady state was established at each sampling time, because the changes in enrichment were relatively small, and the turnover rate of the analyzed intermediates was sufficient to allow almost complete renewal between two sampling times. For example, the turnover time calculated as the ratio of pool size to associated metabolic flux was 0.8, 0.6, and 0.09 h, for the hexose, Glu, and sucrose pools, respectively. Assuming that five turnovers are necessary to renew each intermediate by 97%, the hexose, Glu, and sucrose pools were renewed every 4.0, 3.0, and 0.5 h, respectively. This indicates that the measured enrichments and calculated flux values were representative of the metabolism in the cells at the different stages of culture.

Contrary to most previous studies (18, 20, 25, 26), a relatively long labeling time was necessary to reach the steady state. This suggests the presence of large, slowly exchanging pools in tomato cells: proteins are the most likely candidates, because they are the largest class of cell components (Fig. 2) and they are known to constantly turn over (41). In that case, amino acids from proteins labeled at previous stages would influence the labeling of the free amino acid pool at sampling time. If strong, this memory effect would preclude the use of amino acid labeling, particularly Glu or Asp, as indicators of metabolic fluxes. We evaluated the extent of protein turnover in free amino acid labeling at various stages of the cell culture by a pulse-chase experiment with [^{14}C]Leu (Fig. 7). The specific radioactivity (SR) of free Leu (*f*) and protein Leu (*p*) decreased during the chase between days 3 and 7, indicating active Leu synthesis and protein turnover in cells, with the *f*/*p* ratio remaining constant around 0.5 during the following 3 days. Therefore, the Leu flux from protein degradation (Vd) was equivalent to that of Leu neosynthesis (Vn). Considering the net rate of protein accumulation and the proportion of Leu in proteins, Vn and Vd values at day 5 were 12.4 $nmol \cdot h^{-1} \cdot (10^6 \text{ cells})^{-1}$. The memory effect for Leu is important. The situation is different for Glu because Glu equilibrates with 2-oxoglutarate, an intermediate of the tricarboxylic acid cycle. The flux of 2-oxoglutarate neosynthesis via the tricarboxylic acid cycle was found to be 305 $nmol \cdot h^{-1} \cdot (10^6 \text{ cells})^{-1}$ (Table IV). The flux of Glu from protein degradation is equal to the flux of Glu to the amino acids of the Glu family (Glu, Gln, Arg, and Pro) for protein synthesis, which was found to be 59 or 42 $nmol \cdot h^{-1} \cdot (10^6 \text{ cells})^{-1}$ at day 5, from the steady-state labeling data (Vglu, Table IV) and from the protein composition data, respectively (Table V). The flux of 2-oxoglutarate neosynthesis via the tricarboxylic acid cycle is, therefore, at least 5-fold the Glu flux from protein. This indicates that the free Glu pool contains about 20% of Glu from protein, *i.e.* Glu that had been labeled at previous times. Therefore, protein turnover modifies the labeling of the free Glu pool: in particular, the decrease in the PEPC/PK rate may occur earlier and more quickly than indicated by the increase in the C-3/C-4 ratio (Table II).

Sugar Metabolism—The equations for sugar metabolism in cytosol and plastid (see "Appendix") express the measured enrichments of C-1 of free glucose, and C-1 and C-6 of starch and sucrose glucosyl, to fluxes. Using the enrichment values measured by ^{1}H and ^{13}C NMR, the resolution of 25 equations provided 10 fluxes of sugar metabolism and the theoretical enrichments of glucose C-6 and starch glucosyl C-6 (Table VI). These theoretical enrichment values were not significantly different from the measured enrichments shown in Table I. Therefore, we concluded that our model correctly describes the pathways of sugar metabolism from glucose influx to PEP, including PPP and sucrose cycling.

Oxidative Flux—Our goal was to validate oxidative fluxes, including glycolysis and the tricarboxylic acid cycle. The stoichiometry of NADH production in the intermediary metabolism was used to calculate the O_2 consumption rate. This rate was close enough to the experimental values obtained with the Clark electrode (Table VII) to indicate that the model correctly describes the metabolic network during the culture cycle.

Vpepc Compared with the Flux to Amino Acids of the Asp and Glu Families—To further validate the model, the calculated rates of PEPC flux (Table IV) that correspond to the unidirectional fluxes of biosynthesis (Vglu + Vasp) were compared with the net accumulation rate of amino acid synthesis deriving from 2-oxoglutarate and oxaloacetate, obtained

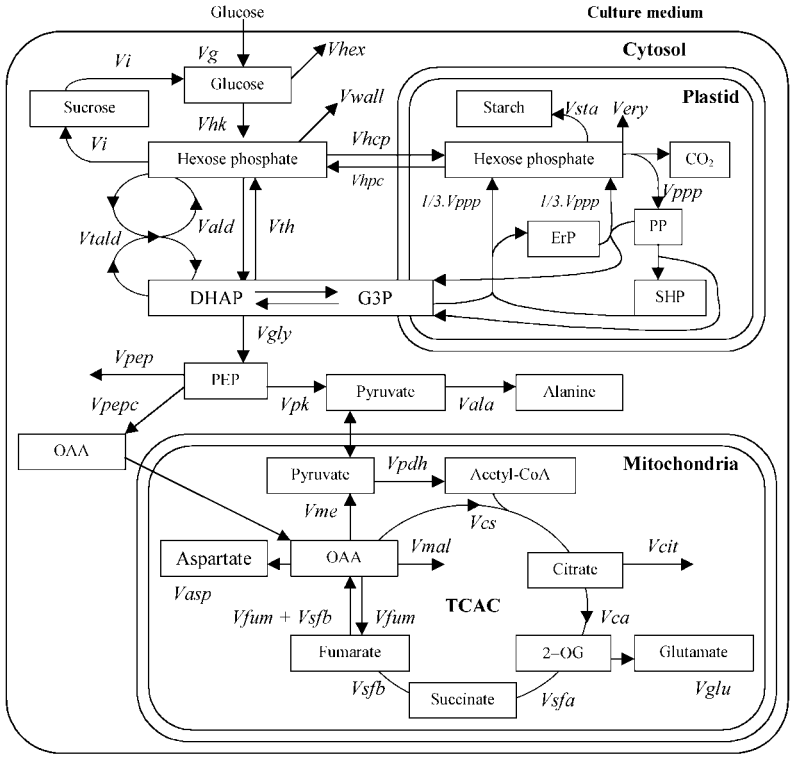

Vg	Glucose influx	Vpk	Oxydative flux through PK
Vhk	Flux into hexose-P pool	Vpepc	Anaplerotic flux through PEPC
Vi	Sucrose synthesis and degradation	Vpdh	Flux through pyruvate DH
Vhex	Soluble sugar accumulation	Vme	Flux through malic enzyme
Vwall	Flux of hexose into wall compounds	Vcs	Flux through citrate synthase
Vald	Unidirectional flux through aldolase	Vca	Flux through aconitase
Vth	Recycling of triose-P to hexose-P	Vsfa	Flux through 2-oxoglutarate DH
Vht	Net flux from hexose-P to triose-P	Vsfb	Flux through succinate DH
Vtald	Cytosolic transaldolase	Vfum	Flux through fumarase
Vgly	Triose-P to PEP	Vpep	Flux to amino-acid production
Vhcp	Hexose-P from cytosol into plastids	Vala	Alanine production
Vhpc	Hexose-P from plastids to cytosol	Vglu	Glutamate production
Vppp	Pentose-P pathway	Vasp	Aspartate production
Vsta	Starch accumulation	Vcit	Citrate accumulation
Very	Flux to amino-acid production	Vmal	Malate accumulation

FIG. 6. **Pathways of carbohydrate metabolism in tomato cells.** Metabolic pathways have been identified by using the labeling of intermediates as described in the text. Flux names are defined under "Appendix." Flux values are given in Table IV.

TABLE III

Conversion factor (F) used to transform the net synthesis rate of protein (Δ prot/Δt, Fig. 2D) into carbon fluxes (Vx) of each amino acid group in tomato cells

Considering the amino acid group composition of the total proteins (AAC) presented in Fig. 3, the average mass of a protein of 100 amino acids (12,600) was determined to express the net synthesis rate of protein (mg protein · h^{-1} · 100 ml^{-1}, Fig. 2*D*) in nmol of protein · h^{-1} · 10^6 cells. Because the mathematical model handles fluxes in nmol carbon · h^{-1} · 10^6 cells, the net synthesis rate of protein (Δprot/Δ*t*) was transformed into these units. (Vx = (Δprot.F)/(Δt.12600) and F = AAC × NC).

Flux (Vx)	Amino acid groups	Amino acid composition of protein in % (AAC)	Number of carbons (NC)	Conversion factor (*F*)
Vglu	Glutamate	20.8	5	104
Vasp	Aspartate	26.8	4	107
Vala	Pyruvate + acetyl CoA	26.6 + 26.8	3	160
Vpep	PEP + 3-PGA	11.8 + 25.7	3	113
Very	Erythrose	5.9	6	35

through the HPLC amino acid analysis in total proteins (Table V). During the exponential phase at day 5, the unidirectional rate of amino acid synthesis for Glu and Asp families (96 ± 7 nmol of hexose equivalent·h^{-1}·(10^6 cells)$^{-1}$, Table IV) was in excess, thus explaining the net accumulation rate of Glu and Asp groups (69 ± 7 nmol of hexose equivalent·h^{-1}·(10^6 cells)$^{-1}$, Table V). Results observed for the cells harvested at days 6 and 7.5 gave good correlation between calculated (unidirectional) fluxes and measured (net accumulation) values (Table V). These different validations indicate that that the model correctly describes the pathways of intermediary metabolism in glucose-fed tomato cells.

Changes in Flux Intensities during the Culture Cycle Are in Contrast with the Stability in Central Metabolic Network

Changes in fluxes in the metabolic network can be analyzed both through absolute and relative flux values (Fig. 6 and Table IV); absolute flux values reflect the activity of cell metabolism, whereas relative values reflect the organization of the metabolic network during the culture cycle.

Exponential Phase (Day 5)—At day 5, 18% of the glucose entering the cells was incorporated into soluble and insoluble sugars (Vhex and Vwall), and 28% (Vhcp − Vhpc) was metab-

TABLE IV

Carbon relative flux and absolute values of metabolic fluxes in tomato cells incubated with [1-^{13}C]glucose at three different physiological conditions

Days of culture and glucose concentration are given for each stage of the culture. Carbon relative flux was calculated by normalizing rates in carbon flux to the rate of carbon glucose influx. Absolute flux is given in nanomoles of hexose equivalent · h^{-1} · $(10^6 \text{ cells})^{-1}$. Flux values calculated from the model based upon carbon enrichment studies are shown as the mean and range of separate simulation using extreme values of enrichments from two independent experiments.

Flux	Exponential phase (day 5) Glucose in medium (90 mM)		Arrest of cell division (day 6) Glucose in medium (65 mM)		Pre-stationary phase (day 7.5) Glucose in medium (30 mM)		Flux description
	Relative carbon flux	Absolute flux	Relative carbon flux	Absolute flux	Relative carbon flux	Absolute flux	
	Ratio	*nmol·h^{-1}·(10^6 cells)$^{-1}$*	*Ratio*	*nmol·h^{-1}·(10^6 cells)$^{-1}$*	*Ratio*	*nmol·h^{-1}·(10^6 cells)$^{-1}$*	
Vg[a]	100 ± 5	602 ± 30	100 ± 5	394 ± 20	100 ± 8	180 ± 14	Glucose influx
Vhk	747 ± 130	4492 ± 782	674 ± 92	2656 ± 362	648 ± 110	1167 ± 198	Flux into hexose-P pool
Vi	653 ± 130	3932 ± 782	592 ± 92	2333 ± 362	553 ± 110	995 ± 198	Sucrose synthesis and degradation
Vhex[a]	7 ± 1	42 ± 3	18 ± 2	71 ± 6	4 ± 2	8 ± 4	Soluble sugar accumulation
Vwall[a]	11 ± 3	67 ± 18	24 ± 5	93 ± 18	0 ± 2	0 ± 4	Flux of hexose into wall compounds
Vald	104 ± 1	625 ± 24	95 ± 2	375 ± 8	113 ± 3	203 ± 5	Unidirectional flux through aldolase
Vth	50 ± 1	299 ± 24	63 ± 2	249 ± 8	53 ± 2	96 ± 4	Recycling of triose-P to hexose-P
Vht	54 ± 1	326 ± 24	32 ± 2	126 ± 6	60 ± 2	107 ± 4	Net flux from hexose-P to triose-P
Vtald	42 ± 20	258 ± 120	46 ± 36	182 ± 110	62 ± 40	110 ± 72	Cytosolic transaldolase
Vgly	67 ± 1	403 ± 8	43 ± 2	168 ± 7	71 ± 1	127 ± 2	Triose-P to PEP
Vhcp	320 ± 25	1925 ± 150	349 ± 20	1373 ± 79	868 ± 11	1562 ± 20	Hexose-P from cytosol into plastids
Vhpc	292 ± 20	1757 ± 120	323 ± 20	1270 ± 79	832 ± 16	1498 ± 28	Hexose-P from plastids to cytosol
Vppp	78 ± 3	465 ± 12	72 ± 6	252 ± 18	66 ± 3	120 ± 6	Pentose-P pathway
Vsta[a]	0 ± 1	0 ± 3	4 ± 2	16 ± 8	12 ± 3	21 ± 5	Starch accumulation
Very[a]	2 ± 0	12 ± 1	1 ± 0	4 ± 1	2 ± 0	3 ± 1	Flux to amino-acid production
Vpk	46 ± 1	278 ± 3	30 ± 2	119 ± 9	56 ± 1	101 ± 2	Oxidative flux through PK
Vpepc	19 ± 1	88 ± 2	12 ± 1	35 ± 1	13 ± 1	17 ± 2	Anaplerotic flux through PEPC
Vpdh	40 ± 1	240 ± 9	28 ± 1	111 ± 4	51 ± 1	91 ± 2	Flux through pyruvate DH[c]
Vme	4 ± 1	17 ± 4	4 ± 2	11 ± 6	3 ± 1	4 ± 2	Flux through malic enzyme
Vcs	80 ± 3	305 ± 18	56 ± 2	136 ± 12	101 ± 2	103 ± 4	Flux through citrate synthase
Vca	79 ± 3	294 ± 18	56 ± 2	136 ± 12	100 ± 2	101 ± 4	Flux through aconitase
Vsfa	58 ± 2	240 ± 9	41 ± 2	111 ± 10	79 ± 1	91 ± 2	Flux through 2-oxoglutarate DH
Vsfb	46 ± 2		33 ± 2		63 ± 1		Flux through succinate DH
Vfum	255 ± 15	1151 ± 67	180 ± 5	532 ± 15	200 ± 5	270 ± 7	Flux through fumarase
Vpep[a]	6 ± 0	38 ± 1	4 ± 0	14 ± 2	5 ± 1	10 ± 2	Flux to amino-acid production
Vala[a]	9 ± 0	54 ± 1	5 ± 0	20 ± 3	8 ± 1	14 ± 2	Alanine production
Vglu[b]	8 ± 1	59 ± 8	5 ± 1	26 ± 4	5 ± 1	10 ± 2	Glutamate production
Vasp[b]	8 ± 1	37 ± 5	5 ± 1	16 ± 3	5 ± 1	6 ± 2	Aspartate production
Vcit[a]	1 ± 0	6 ± 2	0	0 ± 1	1	2	Citrate accumulation
Vmal[a]	0	1	−2 ± 1	−5 ± 2	1	1	Malate accumulation

[a] Fluxes determined directly.
[b] From amino acid analysis of total proteins, the output of carbon was determined to be the same between Vglu and Vasp.
[c] DH, dehydrogenase.

olized inside plastids, but no starch biosynthesis was observed (Fig. 8*A*). In plastids, most of the hexose-P was metabolized through the PPP (Vppp = 78%).

The sucrose cycling flux (Vi) was as high as about 6-fold the glucose influx (Vg). The cytosolic net flux from hexose-P to triose-P (Vht) was 54% of the glucose influx (Fig. 8*A*). Vht was calculated as Vald − Vth, where Vald is the unidirectional aldolase flux and Vth is the recycling of triose-P into hexose-P, the glycolytic flux (Vgly) metabolized 67% of the glucose influx to PEP.

Amino acid synthesis (Vpep, Very, Vala, Vglu, and Vasp) consumed 35% of the glucose entering the cells. The molar ratio Vpk/Vpepc calculated from the absolute values was close to 3, indicating that one triose-P out of four went through the PEPC flux (Table IV). Of the carbon provided by PEPC, 76% was used for the biosynthesis of amino acid of the Glu and Asp families (Vglu and Vasp). The remainder, *i.e.* 20% of the PEPC flux, either went through the malic enzyme reaction, which provided a small fraction (about 5%) of the pyruvate entering the tricarboxylic acid cycle, or led to the accumulation of citric and malic acids.

Arrest of Cell Division (Day 6)—At day 6, the glucose influx value (Vg) was only two-thirds that of day 5. The relative hexose-P flux into plastids remained unchanged (26% of the glucose influx), and the sucrose cycle remained high, at 6-fold the Vg. 42% of the carbon entering the cells was accumulated as soluble and insoluble sugars (Vhex, Vwall). These flux values were twice higher than at day 5 (Fig. 8*B*). The accumulation of starch occurred but was a minor flux (4%) (Fig. 8*B*). These data are in agreement with cytological observations that showed that the increase in FW at this stage was mainly due to cell volume enlargement.

The recycling of triose-P into hexose-P (Vth) increased (63% of the glucose influx), leading to a decrease in the net flux Vht at 32% of the glucose influx (Fig. 8*B*). The relative glycolytic flux (Vgly) dropped to 43% of the glucose influx (Fig. 8*B*). Therefore, the fluxes entering the tricarboxylic acid cycle also diminished in both relative and absolute terms.

Only 20% of the carbon entering cells was used for amino acid synthesis. The ratio Vpk/Vpepc calculated from the absolute values increased to 3.4, indicating that less than one triose-P out of four entered the PEPC flux (Table IV).

Pre-stationary Phase (Day 7.5)—After day 7.5, glucose in the medium was limited to 30 mM, and the glucose consumption rate was about half that on day 6 (Fig. 8*C*). DW accumulation was at its maximum value (Fig. 1), whereas 2.5 more days were necessary to reach the plateau of FW, indicating that the cell growth at this stage was essentially limited to an uptake of

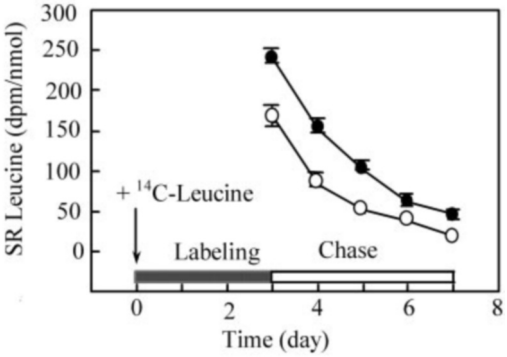

FIG. 7. **Specific radioactivity kinetics of free Leu (○) and protein Leu (●) during the chase of cells incubated for 3 days with [U-^{14}C]Leu.** After 3 days of labeling with [U-^{14}C]Leu (146 kBq.50 ml^{-1}, 10.9 GBq.mmol^{-1}), cells were washed and further incubated in Leu-free medium. Specific radioactivities of free Leu and protein Leu were determined every day as described under "Experimental Procedures." During the chase, the free Leu pool results from the mixture of the fluxes of unlabeled neo-synthesized Leu (Vn), and labeled Leu from protein degradation (Vd), and the resulting Leu were used for protein synthesis (Vs), *i.e.* Leu degradation was considered negligible. At metabolic steady state,Vn + Vd = *Versus*. This gives Vs − Vd = Vn, which is consistent with the fact that the net flux of leu-protein accumulation is equal to Vn. The SR difference between free and protein Leu reflects the recycling of labeled Leu provided by protein turning over into the flux of unlabeled neosynthesized Leu. The equation for metabolic steady state of the Leu pool is Vd**p* = Vs*f, where *p* and *f* are the SR of protein Leu and free Leu, respectively. Because *f*/*p* = 0.5, Vd = 0.5 Vs, and Vn = Vd.

TABLE V

Measured and calculated synthesis rate of amino acids derived from 2-oxoglutarate and oxaloacetate

After acid hydrolysis of total proteins, amino acids were determined by HPLC analysis as described under "Experimental Procedures." Asp and Glu families (Vasp + Vglu) are defined in Fig. 3.

	Synthesis rate of amino acids (Vglu + Vasp)		
	nmol·h^{-1}·(10^6 cells)$^{-1}$		
Day	5	6	7.5
Unidirectional flux	96 ± 7	42 ± 7	16 ± 3
Net accumulation flux	69 ± 7	30 ± 5	18 ± 3

TABLE VI

Calculated enrichments of C-6 hexose and C-6 starch glucosyl in tomato suspension cells

The enrichments were calculated by the model from the measured C-1 enrichments of glucose and starch glucosyl and the C-1 and C-6 of sucrose glucosyl. Results are given as mean ± S.D. (n = 2) and taking into account the extreme values of measured enrichments during labeled experiments.

	^{13}C enrichment		
	%		
Day	5	6	7.5
C-6 hexose	15 ± 1.2	15.8 ± 1.3	16 ± 1.9
C-6 starch glucosyl	18.1 ± 1.1	19 ± 1.1	18.9 ± 1.4

water. The accumulation of starch reached a relatively high rate (12% of Vg), whereas no cell wall polysaccharide biosynthesis was observed. Various relative fluxes (Vppp, Vth, Vgly, and Vpdh) associated to central metabolism remained high and similar to those observed during the exponential growth phase, showing that they are independent from nutritional conditions (Fig. 8). In the same way, the futile sucrose cycle (Vi) remained high at 5.5-fold the Vg.

The relative flux values of anabolic pathways such as anaplerotic flux (Vpepc) or amino acid biosynthesis (Vpep, Very, Vala, Vglu, and Vasp) were similar to those observed at day 6 (Fig. 8), but, due to an increase in Vpk, the ratio Vpk/Vpepc calculated from the absolute values was 5.9, so only one triose-P out of seven went through the PEPC flux (Table IV).

TABLE VII

Calculated and measured consumptions of O_2 in tomato cells

The measured values were obtained by the Clark electrode and the calculated values through the model by taking into account the fact that glycolytic flux (Vgly) produces 2 NADH, Vpdh corresponding to oxidative flux produces 10 NADH equivalent, whereas malic enzyme (Vme) consumes 2 NADH.

	Respiration		
	nmol O_2·h^{-1}·(10^6 cells)$^{-1}$		
Day	5	6	7.5
Calculated	1586 ± 57	712 ± 33	578 ± 14
Measured	1500 ± 200	900 ± 100	600 ± 100

DISCUSSION

The aim of this study was to examine changes in the central metabolism of cultured cells in varying conditions of growth. The quantification of absolute fluxes showed that the activity of metabolism per cell decreased throughout the culture cycle from exponential to early stationary phase, in keeping with the decrease in glucose level in the medium. Surprisingly, measurements of relative flux values showed that the changes in flux rates produced few changes in the organization of the central metabolism network. This provides evidence of the stability of the central metabolism as opposed to the flexibility of the PEPC and other anabolic fluxes.

Validity of the Model—The present method of intracellular flux quantification has been successfully applied to animals (15, 16), microorganisms (17), and plants tissues (18, 20, 25). Steady-state labeling is reached within a few minutes in bacteria and a few hours in animal and plant tissues. In the present case, the labeling time necessary to reach isotopic steady state, *i.e.* 4 days, corresponds to almost two cell generations. These constantly changing conditions could generate no true steady states, and this could be a limitation when quantifying metabolic fluxes.

The validity of the model was confirmed by the correlation between calculated values given by the model and experimental values obtained from independent experiments concerning the C-6 enrichment of free glucose and starch glucosyl (Tables I and VI), the rate of O_2 consumption (Table VII), and the unidirectional fluxes of amino acid synthesis and incorporation into proteins (Tables V and IV).

Despite dramatic changes in the nature of accumulated end-products, the stability of the central metabolism was a surprise, and we excluded two possible artifacts. First the enrichments of intermediates may not reflect the changes in metabolite fluxes if their turnover rate is too slow. By relating measured fluxes to pool sizes, we found that the turnover rates of the major metabolites (hexoses, sucrose, and Glu), were high enough for the measured enrichments at each time to reflect flux changes at the different stages of the culture. The second possible artifact is the memory effect that may result from the labeling and turnover of macromolecules such as proteins or cell wall polysaccharides. This effect may be important here due to both the long labeling time used and a significant turnover rate of these cell components. The introduction of metabolites that had been labeled at a previous period of the culture cycle would hide changes in the central metabolism. We examined the case of proteins, because they are the major component of the cells and their turnover is known to be relatively high compared with cell wall polysaccharides. A labeling experiment with ^{14}C-labeled Leu showed that the proportion of protein-derived amino acids was significant at the different stages of the culture cycle examined here, but probably not high enough to hide strong changes in flux values. Indeed, a decrease in the enrichment at Glu C-2 and C-3 with C-4 was observed at day 7.5, because the growth

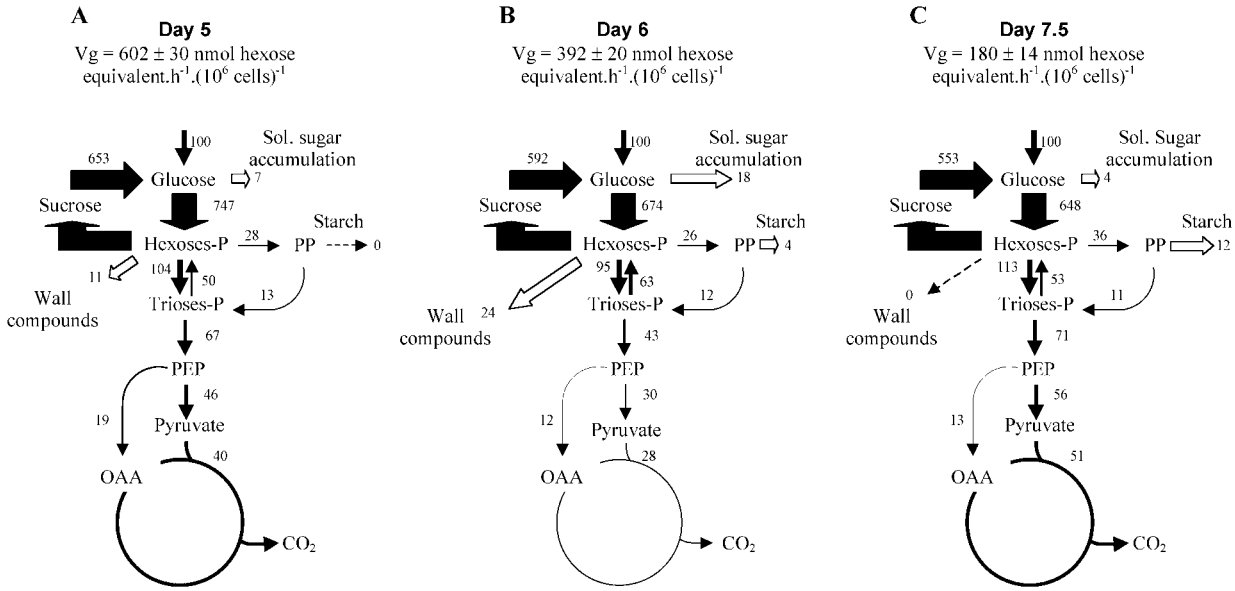

FIG. 8. **Stability of central metabolism and flexibility of end-product anabolic pathway at various stages of the culture cycle.** *A*, during exponential growth phase (day 5); *B*, during arrest of cell division phase (day 6), and *C*, pre-stationary phase (day 7.5). Abbreviations are the same as in Fig. 6. The *numbers* indicate carbon relative fluxes calculated by normalizing rates in carbon fluxes to the rate of glucose influx (Vg).

rate decreased (Table II). The memory effect may become stronger when the rate of protein degradation increases. In the present case, the protein level kept increasing and at day 7.5 remained constant. This measurement of protein turnover is consistent with previous data on global protein turnover in plants (42). The situation may be different when protein degradation is stimulated, as occurs during stresses or sugar starvation (43). In conclusion, we argue that our data give a reliable picture of the metabolism network in plant cells during a growth cycle.

Stability of Central Metabolism and Futile Cycles during the Cell Culture Cycle—The central pathways (glycolysis, tricarboxylic acid cycle, and PPP) supply the metabolites and energy necessary for growth and maintenance. The relative flux values associated with the central metabolism (Vgly, Vppp, and Vpdh) remained remarkably constant during the growth cycle (Fig. 8 and Table IV), with ~70% of entering glucose and ~70% of the oxidative PPP (Table IV) passing through glycolysis. The only changes in the relative fluxes observed in the central metabolic pathways occurred on day 6 during the transition between active and resting cells (Fig. 8 and Table IV), where Vgly and Vpdh were only two-thirds of that on day 5 or day 7.5. These results illustrate the stability of the central metabolism through the culture cycle. Similarly, the switch from sucrose and starch synthesis to sucrose and starch degradation in *Chenopodium rubrum* and sugar beet cells occurred without any significant increase in respiration (44, 45).

Two futile cycles associated with the central metabolic pathways were observed. One was the release of the glucosyl moiety of hexose phosphates or sucrose to free glucose, which may be due to either the hydrolysis of sucrose by an invertase or to the dephosphorylation of glucose phosphates by a phosphatase. As in a previous work (20), the preferred hypothesis is sucrose hydrolysis, because there has been no evidence for glucose phosphate phosphatase, although evidence for hexose phosphate phosphatase active on methyl-glucose phosphate was recently obtained in maize root tips (46). The other one is cycling between triose-P and hexose-P (Fig. 8). During the exponential phase of growth, the rate of sucrose cycling was 6-fold the unidirectional flux of entering glucose (Fig. 8 and Table IV). The presence of rapid sucrose turnover involves some apparent wastage of energy (20, 23). Sucrose synthesis consumes between 1 and 2 ATP molecules per hexose-P depending on the enzyme implicated in sucrose synthesis (sucrose synthase or sucrose phosphate synthase) (46). From the rate of NADH production and assuming that the P/O ratio was 3, the maximum rate of ATP synthesis during the exponential phase was between 15.2 and 9.5 μmol of ATP·h^{-1}·(10^6 cells)$^{-1}$. At day 5, the sucrose cycle consumed 5.9 ± 2 μmol of ATP·h^{-1}·(10^6 cells)$^{-1}$, which corresponds to 62 ± 20% of the ATP produced by mitochondrial respiration. The sugar accumulation observed at the end of the exponential phase (day 6) was associated with a high sucrose turnover (Table IV), consuming 82 ± 27% of total ATP production. In the pre-stationary phase, sucrose turnover consumed 43 ± 14% of total ATP produced by cells. The high fluxes of sucrose cycling found here are consistent with those found in ripening bananas (23) and in maize root tips (20). Possible roles for this futile cycle include the following: maintaining the balance between the accumulation of sucrose and the demand for carbon for respiration and biosynthesis in the cell (45, 47, 48) or the regulation of the sucrose and hexose concentrations in relation to the water status of the cell (20). It is interesting to note that the rate of sucrose cycling was closely related with glucose influx (around 6-fold) but in no case with alterations in hexose or starch accumulation. The sucrose cycle contributes to an active recycling of hexose-P and soluble sugars, thus generating a unique pool of sugars.

The comparison of metabolic flux values in tomato cells with those in corn root tips (20), banana fruits (23), and *C. rubrum* and sugarcane cells (44, 45) offers the first opportunity to explore the metabolic flux stability in plant cells. In the maturing banana, an active starch-to-hexose conversion has been observed without any growth (23). In corn root tips the intermediary metabolism was found to be more active than in tomato cells (20), and a high proportion (75%) of the glucose entering the root tips was used in the non-triose pathways, including a high flux of polysaccharide synthesis (20). Despite these differences, a number of similarities in central metabolism flux values are to be noted. In these two types of cell, PPP flux (Vppp) and the recycling of triose-P to hexose-P (Vth) consumed, respectively, 28 and 40% of the glucose entering the

cell (Fig. 8 and Table IV). A similarly high activity of the oxidative pentose phosphate pathway was found in maize root tips (20), and in cells of *C. rubrum* (47) and *Daucus carota* (48). A considerable recycling of triose phosphate in the cytosol has also been observed in *C. rubrum* cells and potato tubers (44) and an active futile cycle of sucrose in sugarcane (45), corn root tips (20), maturing banana (23), and kiwifruit (49), but lower values were found in *C. rubrum* cells (44).

The stability of the central metabolism (glycolysis, tricarboxylic acid cycle, and PPP) and associated futile cycles (turnover of sucrose and triose-P recycling) can be explained by the fact that these fluxes are fast compared with end-product accumulation, and most of the ATP was not consumed by biosynthetic or transport processes, but by the turnover of sucrose, which appears to be subject to the rate of glucose absorption. The central metabolism has evolved coordination of pathway control to maintain a central pool of the main intermediary metabolites (soluble sugars, hexose-P, UDP-glucose, and triose-P). The fluxes in the central pathways were fast enough compared with those in anabolic pathways to readjust intermediary metabolite levels instantly in the network. These results suggest that the control architecture for the synthesis of cellular compounds prevents alteration of central metabolic fluxes during the growth of cells and could explain the flexibility of plant metabolism.

Flexibility of Anabolic Fluxes Related to Sugar Nutrition during the Cell Culture Cycle—In this study, the accumulation of starch (Vsta), soluble sugar (Vhex), wall polysaccharides (Vwall), and amino acid biosynthesis (Vasp + Vglu + Vala + Vpep + Very) were the major anabolic pathways. These anabolic fluxes were small compared with those in the central metabolism and highly variable, thus providing the flexibility to meet the cell needs. At day 5, transient modifications in carbon metabolism were observed in relation to the interruption of cell division. The cells started to accumulate free hexoses and produce more wall polysaccharides (Vhex and Vwall, Fig. 8 and Table IV) concomitantly with an increase in cell volume and an uptake of water (Fig. 1). Twenty-four hours later, the entering hexoses were preferentially stored in the form of starch (Vsta, Fig. 8 and Table IV).

The function of PEPC is to provide carbon skeletons for the net biosynthesis of amino acids of the Asp and Glu families, and organic acids. The net flux to organic acids in tomato cells during a growth cycle was a minor one (Table IV). The relative activity of PEPC and PK, the two major branches for the output of glycolysis, have been compared in different growing tissues. The Vpk/Vpepc ratio is highly variable. In sugar-fed maize root tips (20, 24) and developing soybean seeds (50) as in tomato cells in exponential phase (this study), the Vpk/Vpepc ratio was around 3, which means that three-fourths of triose-P provided by glycolysis were found to be directed through the pyruvate kinase and one-fourth through the PEP branch. In barley aleurone layers, the Vpk/Vpepc ratio was 0.6 in developing seeds but decreased by a factor of 3–5 in aleurone layers of mature seeds that secrete malic acid into the endosperm (51). On the other hand, the Vpk/Vpepc ratio increased from 3 to 6 during the growth cycle of tomato cells. This slowing down of the PEPC flux could be compared with the interruption of this flux observed in corn root tips after 6 h of carbon starvation (25). The decrease in the PEPC flux during the growth cycle may be reversed by addition of fresh medium, as shown by enrichments of Glu carbons similar to those observed at days 5 or 6 (result not shown). This observation suggests that the PEPC activity was related to the supply of sugars to the cell. The mechanisms used by tomato cells to control the PEPC flux during the growth cycle are under investigations.

In conclusion, these results show that the metabolic network of plant cells is organized in two distinct but coordinated sets of pathways. In the central metabolic pathways (glycolysis, PPP, and tricarboxylic acid cycle) flux rates are highly dependent on nutritional conditions, but relative fluxes are mainly constant, *i.e.* the structure of this set of reactions remains constant. These pathways contribute to the production of energy and intermediary metabolites necessary for cellular biosyntheses. The associated futile cycles increase the efficiency of exchanges between the different metabolite pools, thus providing stability to the central metabolism. On the contrary, anabolic pathways both in absolute and relative terms have small and highly variable fluxes that adjust cellular biosyntheses to environmental conditions.

Acknowledgments—We thank Dr. Albert de Graaf (University of Juelich, Germany) for the critical reading of the manuscript, Mickael Maucourt for his dedicated technical assistance with NMR spectrometry and plant cell cultures, Monique Gaudillère for her assistance with HPLC metabolite measurements, Marian Mouassite for [U-^{14}C]Leu labeling experiments, and Sarah Julienne for cytological observations.

APPENDIX

Our model shown in Fig. 6 was used to estimate 29 fluxes. The glucose influx into cells (Vg) was determined directly by monitoring the glucose decrease in medium during the culture cycle (Fig. 1*A*). Ten net fluxes as accumulation of sugars (Vhex), starch (Vsta), cell wall polysaccharides (Vwall), organic acids (Vcit and Vmal), and biosynthetic pathways of amino acids (Very, Vpep, Vala, Vglu, and Vasp) were calculated after measuring metabolite levels experimentally. Eighteen fluxes of intermediary metabolism in futile cycle (Vi), glycolysis (Vhk, Vth, Vald, Vtald, Vgly, and Vpk), pentose-P pathway (Vppp, Vhcp, and Vhpc), tricarboxylic acid cycle (Vpdh, Vcs, Vca, Vsfa, Vsfb, Vfum, and Vme), and anaplerotic pathway (Vpepc) were calculated by using a metabolic labeling approach (24).

Flux of Sugar Metabolism in Cytosol and Plastid—The carbon fluxes were as in Fig. 6. For cytosol: Vg, flux of glucose inflow into the cultured cells; Vi, flux of synthesis and degradation of sucrose via sucrose-P synthase and invertase; Vwall, flux of hexose into wall compounds; Vhex, flux of hexoses accumulation; Vhk, flux of glucose into the hexose-P pool; Vald, unidirectional flux through aldolase reaction; Vth, resynthesis of hexose-P from triose-P; Vht, net flux of hexose-P to triose-P (Vald − Vth); Vtald, exchange of the C4 to C6 moiety of cytosolic fructose-P and free triose-P through the cytosolic transaldolase reaction; Vgly, flux of triose-P to PEP. For plastid: Vcp, net flux of hexose-P transport from cytosol to plastid (Vcp = Vhcp − Vhpc with Vhcp, hexose-P transport from cytosol to plastid and Vhpc, hexose-P transport from plastid to cytosol); Vsta, synthesis of starch; Vppp, flux of pentose-P pathway; Very, amino acid production (phenylalanine, tyrosine, and tryptophane) from erythrose-P (to simplify the equation, Very leaves the hexose-P taking in account the carbon correction output); PP, pentose-P; SHP, sedoheptulose-7-P; ErP, erythrose-P; DHAP, dihydroxyacetone-P; G3P, glyceraldehyde-3-P; PEP, phosphoenol-pyruvate.

All Vi rates are given as relative carbon flux at isotopic steady state as follows: G1m-G6m, medium glucose carbon; G1–6, cellular glucose carbon; P1–6, pentose-P carbon; HP1–6, plastid hexose-P carbon; H1–6, hexose-P carbon; T1–3, triose-P carbon.

Enrichments of glucose: G1*(Vg + Vi) = G1m*Vg + H1*Vi; G2*(Vg + Vi) = G2m*Vg + H2*Vi; G3*(Vg + Vi) = G3m*Vg + H3*Vi; G4*(Vg + Vi) = G4m*Vg + H4*Vi; G5*(Vg + Vi) = G5m*Vg + H5*Vi; G6*(Vg + Vi) = G6m*Vg + H6*Vi.

Enrichments of pentose-P: P1 = HP2, P2 = HP3, P3 = HP4, P4 = HP5, P5 = HP6.

Enrichments of cytosolic hexose-P: H1*(Vhk + Vth + Vhpc) = G1*Vhk + T3*Vth + HP1*Vhpc; H2*(Vhk + Vth + Vhpc) = G2*Vhk + T2*Vth + HP2*Vhpc; H3*(Vhk + Vth + Vhpc) = G3*Vhk + T1*Vth + HP3*Vhpc; H4*(Vhk + Vth + Vhpc + Vtald) = G4*Vhk + T1*Vth + HP4*Vhpc + T1*Vtald; H5*(Vhk + Vth + Vhpc + Vtald) = G5*Vhk + T2*Vth + HP5*Vhpc + T2*Vtald; H6*(Vhk + Vth + Vhpc + Vtald) = G6*Vhk + T3*Vth + HP6*Vhpc + T3*Vtald.

Enrichments of plastidial hexose-P: HP1*(Vhcp + (2/3)*Vppp) = H1*Vhcp + (2/3)*P1*Vppp; HP2*(Vhcp + (2/3)*Vppp) = H2*Vhcp + (2/3)*P2*Vppp; HP3*(Vhcp + (2/3)*Vppp) = H3*Vhcp + (1/3)*P2*Vppp + (1/3)*P1*Vppp; HP4*(Vhcp + (2/3)*Vppp) = H4*Vhcp + (1/3)*P3*Vppp + (1/3)*T1*Vppp; HP5*(Vhcp + (2/3)*Vppp) = H5*Vhcp + (1/3)*P4*Vppp + (1/3)*T2*Vppp; HP6*(Vhcp + (2/3)*Vppp) = H6*Vhcp + (1/3)*P5*Vppp + (1/3)*T3*Vppp.

Enrichments of triose-P: T1*(2*Vald + (2/3)*Vppp + Vtald) = (H3 + H4)*Vald + (2/3)*P3*Vppp + H4*Vtald; T2*(2*Vald + (2/3)*Vppp + Vtald) = (H2 + H5)*Vald + (2/3)*P4*Vppp + H5*Vtald; T3*(2*Vald + (2/3)*Vppp + Vtald) = (H1 + H6)*Vald + (2/3)*P5*Vppp + H6*Vtald.

Input-output glucose: Vg + Vi = Vhk + Vhex. Input-output hexoses-P cytosolique: Vhk + Vth + Vhpc = Vi + Vald + Vhcp + Vwall. Input-output hexose-P plastidial: Vhcp + (2/3)*Vppp = Vhpc + Vppp + Vsta + Very. Input-output triose-P: Vald + (1/3)*Vppp = Vgly + Vth + (1/6)*Vppp.

Flux of PEP Metabolism and Tricarboxylic Acid Cycle—The carbon fluxes were as in Fig. 6. For cytosol: Vgly, flux of triose-P to PEP; Vpep, amino acid production (Phe, Tyr, Trp, Ser, Gly, Cys, Met, Fig. 3) from PEP and 3-PGA; Vpepc, flux through the phosphoenolpyruvate carboxylase; Vpk, flux through the pyruvate kinase; Vala, amino acids (Ala, Val, Leu, Lys, Fig. 3) production from Ala and pyruvate (to simplify the equations the carbon leaves only the pyruvate, taking into account the carbon correction output). For mitochondria: Vpdh, flux through pyruvate dehydrogenase; Vcs, flux through citrate synthase; Vca, flux through aconitase and isocitrate dehydrogenase; Vsfa, flux through 2-oxoglutarate dehydrogenase and succinyl-CoA synthetase; Vsfb, flux through succinate dehydrogenase; Vfum, flux through fumarase dehydratase; Vme, flux through malic enzyme; Vglu, amino acid production (Glu, Gln, Arg, Pro, Fig. 3) from 2-oxoglutarate; Vasp, amino acid production (Asp, Asn, Thr, Ile, Met, Lys, Fig. 3) from oxaloacetate; Vcit and Vmal, citrate and malate accumulation. (OAA, oxaloacetate; 2-OG, 2-oxoglutarate; 3-PGA, 3-phosphoglycerate.)

All Vi rates are given as relative carbon flux at isotopic steady state as follows: E1–3, PEP carbon; Py1–3, pyruvate carbon; A1–2, acetyl-CoA carbon; O1–4, OAA carbon; S1–2, succinate carbon (S2 for the 2 central carbon); F1–2, fumarate carbon (F2 for the 2 central carbon).

Enrichments of pyruvate: Py1*(Vpk + (3/4)*Vme) = E1*Vpk + O1*Vme*(3/4); Py2*(Vpk + (3/4)*Vme) = E2*Vpk + O_2*Vme*(3/4); Py3*(Vpk + (3/4)*Vme) = E3*Vpk + O3*Vme*(3/4).

Enrichments of acetylCo: A1 = Py2, A2 = Py3.

Enrichments of OAA: O1*(Vpepc + Vsfb + Vfum) = E1*Vpepc + F1*(Vsfb + Vfum); O_2*(Vpepc + Vsfb + Vfum) = E2*Vpepc + F2*(Vsfb + Vfum); O3*(Vpepc + Vsfb + Vfum) = E3*Vpepc + F2*(Vsfb + Vfum); O4*(Vpepc + Vsfb + Vfum) = E4*Vpepc + F1*(Vsfb + Vfum).

Enrichments of succinate: S1 = (A1 + O3)*0.5, S2 = (A2 + O2)*0.5.

Enrichments of fumarate: F1*(Vsfb + Vfum) = S1*Vsfb + (O1 + O4)*0.5*Vfum; F2*(Vsfb + Vfum) = S2*Vsfb + (O2 + O3)*0.5*Vfum.

Input-output PEP: Vgly = Vpk + (3/4)*Vpepc + Vpep. Input-output pyruvate: Vpk + (3/4)*Vme = Vpdh + Vala. Input-output citrate: Vcs = 2*Vpdh, Vcs = Vcit + Vca. Input-output 2-OG: (5/6)*Vca = Vglu + Vsfa. Input-output succinate: (4/5)*Vsfa = Vsfb. Input-output OAA: Vpepc + Vsfb = Vme + (4/6)*Vcs + Vasp + Vmal.

Converting relative fluxes to absolute fluxes: Vg, Vhk, Vi, Vhex, Vwall, Vald, Vth, Vht, Vtald, Vgly, Vhcp, Vhpc, Vppp, Vsta, Very, Vgly, Vpk, Vpdh, Vala, and Vpep are converted by the following relation: $V^{abs} = P*(1/6)*V^{rel}$; Vpepc, Vme, Vasp, and Vmal: $V^{abs} = P*(3/4)*(1/6)*V^{rel}$; Vglu: $V^{abs} = P*(1/5)*V^{rel}$; Vcit: $V^{abs} = P*(1/6)*V^{rel}$; $P = (Vg^{abs} \times 6)/100$. Vg^{abs} is measured by the decreased level of glucose in the culture medium. P values are 36.1, 23.6, and 10.8 for d5, d6 and d7.5 respectively.

REFERENCES

1. Smirnoff, N. (1995) in *Environment and Plant Metabolism: flexibility and acclimation* (Smirnoff, N., ed) pp. 1–16, Bios Scientific Publishers, Oxford
2. ap Rees, T., and Hill, S. A. (1994) *Plant Cell Environ.* **17,** 587–599
3. Plaxton, W. C. (1996) *Ann. Rev. Plant Physiol. Plant Mol. Biol.* **47,** 185–214
4. Stitt, M., (1994) *Curr. Opin. Biotech.* **5,** 137–143
5. Stitt, M., and Sonnewald, U. (1995) *Annu. Rev. Plant Physiol. Plant Mol. Biol.* **46,** 341–368
6. Herbers, K., and Sonnewald, U. (1996) *Tibtech* **14,** 198–205
7. Gottlob-McHugh, S. G., Sangwan, R. S., Blakeley, S. D., Vanlerberghe, G. C., Ko, K., Turpin, D. H., Plaxton, W. C., Miki, B. L., and Dennis, D. T. (1992) *Plant Physiol.* **100,** 820–825
8. Hajirezaei, M., Sonnewald, U., Viola, R., Carlisle, S., Dennis, D., and Stitt, M. (1994) *Planta* **192,** 16–30
9. Zrenner, R., Krause, K.-P., Apel, P., and Sonnewald, U. (1996) *Plant J.* **9,** 671–681
10. Schaaff, I., Heinisch, J., and Zimmermann, F. K. (1989) *Yeast* **5,** 285–290
11. Davies, S. E. C., and Brindle, K. M. (1992) *Biochemistry* **31,** 4729–4735
12. Nuccio, M. L., Russel, B. L., Nolte, K., D., Rathinasabapathi, B., Gaye, D. A., and Hanson, A. D. (1998) *Plant J.* **16,** 101–110
13. McNeil, S. D., Rhodes, D., Russell, B. L., Nuccio, M. L., Shachar-Hill, Y., and Hanson, A. D. (2000) *Plant Physiol.* **124,** 153–162
14. Stephanopoulos, G., and Vallino, J. J. (1991) *Science* **252,** 1675–1681
15. Malloy, C. R., Sherry, A. D., and Jeffrey, M. H. (1988) *J. Biol. Chem.* **263,** 6964–6971
16. Bouzier, A.-K., Goodwin, R., de Gannes, F. M., Valeins, H., Voisin, P., Canioni, P., and Merle, M. (1998) *J. Biol. Chem.* **273,** 27162–27169
17. Marx, A., de Graaf, A. A., Wiechert, W., Eggeling, L., and Sahm, H. (1996) *Biotechnol. Bioeng.* **49,** 111–129
18. Salon, C., Raymond, P., and Pradet, A. (1988) *J. Biol. Chem.* **263,** 12278–12287
19. Martin, F., Boiffin, V., and Pfeffer, P. E. (1998) *Plant Physiol.* **118,** 627–635
20. Dieuaide-Noubhani, M., Raffard, G., Canioni, P., Pradet, A., and Raymond, P. (1995) *J. Biol. Chem.* **270,** 13147–13159
21. Roscher, A., Emsley, L., Raymond, P., and Roby, C. (1998) *J. Biol. Chem.* **273,** 25053–25061
22. Roscher, A., Kruger, N. J., and Ratcliffe, R. G. (2000) *J. Biotech.* **77,** 81–102
23. Hill, S. A., and ap Rees, T. (1994) *Planta* **192,** 52–60
24. Katz, J., and Rognstad, R. (1967) *Biochemistry* **6,** 2227–2247
25. Dieuaide-Noubhani, M., Canioni, P., and Raymond, P. (1997) *Plant Physiol.* **115,** 1505–1513
26. Edwards, S., Nguyen, B.-T., Do, B., and Roberts, J. K. M. (1998) *Plant Physiol.* **116,** 1073–1081
27. Murashige, T., and Skoog, F. (1962) *Physiol. Plant.* **15,** 473–497
28. Stitt, M., and ap Rees, T. (1978) *Phytochemistry* **17,** 1251–1256
29. Moing, A., Escobar-Gutiérrez, A., and Gaudillère, J.-P. (1994) *Plant Physiol.* **106,** 591–600
30. Kunst, A., Draeger, B., and Ziegenhorn, J. (1984) in *Methods of Enzymatic Analysis* (Bergmeyer, H. U., ed) Vol. 6, 3rd Ed., pp. 163–172, Verlagchemie, Weinheim
31. Mollering, H., and Gruber, W. (1966) *Anal. Biochem.* **17,** 369–376
32. Cohen, S. A., and De Antonis, K. M. (1994) *J. Chromatogr.* **661,** 25–34
33. Brouquisse, R., James, F., Pradet, A., and Raymond, P. (1992) *Planta* **188,** 384–395
34. Rance, M., and Byrd, R. A. (1983) *J. Magn. Reson.* **52,** 221–240
35. Kanabus, J., Bressan, R. A., and Carpita, N. C. (1986) *Plant Physiol.* **82,** 363–368
36. Botha, F. C., and O'Kennedy, M. M. (1998) *Physiol. Plant.* **102,** 429–436
37. Ireland, R. (1997) in *Plant Metabolism* (Dennis, D. T., Turpin, D. H., Lefebvre, D. D., and Layzell, D. B., eds) 2nd Ed., pp. 478–494, Addison Wesley Longman, England
38. Bryan, J. K. (1992) in *Biochemistry of Plants: A Comprehensive Treatise* (Stumpf, P. K., and Conn, E. E., eds) Vol. 5, pp. 403–452, Academic Press Inc., New York
39. Flugge, U. I. (1998) *Curr. Opin. Plant. Biol.* **1,** 201–206
40. Weber, A., Servaites, J. C., Geiger, D. R., Kofler, H., Hille, D., Groner, F., Hebbeker, U., and Flugge, U. I. (2000) *Plant Cell* **12,** 787–802
41. Lozovaya, V. V., Zabotina, O. A., and Widholm, J. M. (1996) *Plant Physiol.* **111,** 921–929
42. Davies, D. D., (1982) in *Encyclopedia of Plant Physiology Nucleic Acids and*

Proteins in Plants (Boulter, D., and Parthier, B., eds) Vol. 14, pp. 189–227, Springer-Verlag, Berlin
43. Brouquisse, R., James, F., Raymond, P., and Pradet, A. (1991) *Plant Physiol.* **96,** 619–626
44. Hatzfeld, W.-D., and Stitt, M. (1990) *Planta* **180,** 198–204
45. Wendler, R., Veith, R., Dancer, J., Stitt, M., and Komor, E. (1990) *Planta* **183,** 31–39
46. Cortez, S., Gromova, M., Evrard, A., Roby, C., Heyraud, A., Rolin, D., Raymond, P., and Brouquisse, R. (2002) *Plant Physiol.* (in press)
47. Dancer, J., Hatzfeld, W.-D., and Stitt, M. (1990) *Planta* **182,** 223–231
48. Krook, J., Vreugdenhil, D., Dijkema, C., and van der Plas, L. H. W. (1998) *J. Exp. Bot.* **49,** 1917–1924
49. MacRae, E., Quick, W. P., Benker, C., and Stitt, M. (1992) *Planta* **188,** 314–323
50. Adams, C. A., Broman, T. H., and Rinne, R. W. (1982) *Plant Cell Phyiol.* **23,** 959–965
51. Macnicol, P. K., and Raymond, P. (1998) *Physiol. Plant.* **103,** 132–138